INCLUSION DISTRIBUTION IN INGOTS - A GUIDE TO SEGREGATION MECHANISM

M.D.Maheshwari, T.Mukherjee and J.J. Irani
Tata Iron & Steel Co.Ltd., Jamshedpur

The metling point of non-metallic inclusions, and their nature and distribution can be a guide in deciphering the mode of solidification and segregation in an ingot. A commercial ingot was sectioned, and examined microscopically. Inclusion identification was carried out by optical method as well as by electron probe micro analysis. The extent of segregation was obtained by extensive spectrochemical analysis. It has been found that the shape and position of bottom cone of negative segregation coincide with that of bottom cone of inclusions. A theory of ingot segregation has been put forward on the basis of these results. It has been suggested that the bottom cone of oxide inclusions is a result of incorporation of these inclusions in the dendrites of equiaxed grains. The inclusions drop to the bottom end with the shower of relatively pure equiaxed grains.

While the interdendritic fluid is enriched in elements like C, Mn, S, P, it is denuded of oxygen. Since the oxygen solubility is low, oxygen enrichment leads to immediate precipitation of oxides.

INTRODUCTION

Microsegregation is a manifestation of the dendritic nature of solidification. Fundamentally, it comprises the coring effect in the dendrite and the difference in chemical analysis between the dendrite and the interdendritic region. There is a general consensus about the theories of microsegregation and many good reviews(1-14) are available on this subject. Macrosegregation invariably involves movement of solute rich liquid within the liquid/solid zone. This movement may be attributed to density differences arising out of concentration differences and/or due to temperature variations or for feeding contractions either due to thermal reasons or due to phase transformations. It has been well established that interdendritic flow plays an important role in determining the overall macrosegregation patterns in solidifying ingots.(8,11,15-18) The essential characteristics of this segregation pattern are two zones of positive segregation, one having a shape of a trunkated 'A' situated between the columnar and equiaxed zone (A segregates) and one having the shape of a 'V' situated in the central upper portion of the ingot ('V' segregates). In addition there is a zone of cone shaped negative segregation situated in the lower axial portion of the ingot. The 'A' segregates have been explained as the manifestation of chanelled flow in the interdendritic regions of the columnar zone(15,19) where as 'V' segregates, which appear late in the solidification process, are apparently a consequence of the general settling of crystals in the equiaxed zone(18,20). The region of high purity material at the bottom of the ingot has been attributed to the gravity segregation of primary dendrites formed by dendrite remelting in the columnar zone(21) or by nucleation on inclusions(22,23) and also to constrained convective fluid flow(21). Although several theories (15-36) have been advanced to explain the origin of different types of macrosegregation, unanimity of views on all aspects of the segregation pattern has still not been reached. During the past few

years, several investigations(37-40) had been undertaken at the Tata Iron and Steel Company Limited to study the nature, size and distribution of inclusions in semi finished and finished products as part of a general programme for identifying origins of different defects in the products manufactured at the authors' works. Results of these investigations indicated that the shape, nature, size, distribution and melting point of inclusions can be a significant guide for determining the mode of solidification and origin of macroscopic segregation. Based on these observations, an investigation was undertaken at the authors' works to study the mechanism of macrosegregation patterns in steel ingots. The paper puts forward a hypothesis to explain some aspects of macroscopic segregation patterns in killed steel ingots.

EXPERIMENTAL

The ingots selected for detailed examination were of aluminium silicon killed carbon-manganese steel. The ladle sample analysis varied in the following range:-

Carbon	- 0.48/0.58%
Manganese	- 0.65/0.80%
Silicon	- 0.17/0.30%
Sulphur	- 0.022/0.031%
Phosphorus	- 0.023/0.034%

Steel was made in 90 tonne capacity stationary basic open hearth furnace. Standard procedures were adhered to for charge compositions, melt-out carbon, tapping temperatures etc. The 2.2 tonnes ingots were bottom poured in wide-end-up, duo-decagonal moulds (375 mm diameter) fitted with conventional hot tops and treated with proprietary bottom pouring compound. The details of heat making and teeming are given in Table I. Ladle sample analysis of experimental heats is given in Table II. Approximate chemical analysis of bottom pouring compound is given in Table III. Ingots were stripped after 8 hours of end teeming and identified for detailed investigation. Because of the very extensive and time consuming nature of the investigation, it was decided to examine thoroughly one such ingot. The bottom portion of two more ingots was studied in detail. Ladle sample analysis of these ingots are also given in Table II.

SAMPLING PROCEDURE

Liquid metal and the slag samples were taken at intervals during the refining period. Slag analysis are given in Table I. To eliminate the chances of the inclusions becoming more aluminous, the metal samples were not killed by aluminium. The ingot was sectioned both horizontally and vertically (Fig.1). It was assumed that the ingot structures were symmetrical about the central axis. Therefore, the examination was restricted to one half of the ingot. These pieces (Fig.1) were macro etched and sulphur printed and then sectioned into thin strips; the strips were cut to provide specimens suitable for microscopical examination and subsequent scanning electron microscopy and micro analysis. The samples were polished in diamond paste on Strüer's wheels and etched in various reagents to study the position of inclusions in the macrostructure.

Micro examination and photography were mainly done on a Zeiss Ultraphot microscope. The scanning electron microscope was of Philips make, PSEM 500, with built in LINK, Edax micro analysis facilities using energy dispersal principles. Quantitative analysis was done with ZAF corrections, using cobalt as standard. The piece of polished pure cobalt was attached to the sample by conducting vacuum plasticine (compound) and kept at the same level as the sample. The filament voltage was 25 KV, and the beam size used was 640 A°. The size of area energised for micro analysis under these conditions was 1 μ. The combination of PSE, PSEM 500 and the LINK system allowed X-ray photography for different elements.

Quantitative assessments of the volume fraction of oxide and sulphide inclusions were made on each of the samples by point counting method.(41)

The metallographic sample, polished in the normal manner, was viewed on the microscope at X 500 or X 1000 magnification with a grid superimposed on the eye piece. The grid had 400 intercepts. The intercepts which were coincident with the inclusion image were counted. The process was repeated for hundred independent fields. The volume fraction was obtained by dividing the average number of coincident intercepts per field by the total number of intercepts on the grid i.e.400. Chemical analysis of samples from bottom portion of ingots

TABLE I - CAST DETAILS

Charge Composition

Material	Weight (tonnes) Cast No. A 11876	Cast No. A 12997
Scrap	40.50	40.10
Hot metal	42.50	43.50
Iron ore	1.00	nil
Lime stone	7.00	8.30
Hot metal analysis		
Si (%)	1.68	1.78
S (%)	0.037	0.030
Mn (%)	0.67	0.74

Log of heats

Opening carbon (%)	1.15	1.18
Carbon drop (% carbon/min.)	0.431	0.369
Analysis of first slag sample (%)		
CaO	38.60	39.72
MgO	6.10	6.21
SiO_2	21.18	20.24
FeO	9.10	9.70
P_2O_5	3.27	3.21
S	0.05	nil
Al_2O_3	4.23	3.97
MnO	12.28	12.91
TiO_2	2.10	2.50
Analysis of last steel sample (10 minutes before tap)		
C (%)	0.52	0.56
Mn (%)	0.28	0.28
Analysis of last slag sample		
CaO	42.80	41.97
MgO	6.40	6.81
SiO_2	18.80	19.30
FeO	9.10	9.90
P_2O_5	2.43	2.71
S	0.04	0.01

Table I contd....

	Cast No. A 11876	Cast No. A 12997
Al_2O_3	3.30	3.37
MnO	10.55	11.10
TiO_2	2.10	2.10
Bath temperature ^oC	1560 (10 minutes before tap)	1555 (2 minutes before tap)
Deoxidisers		
Bath		
Ferro-manganese	800 kg (10 minutes before tap)	800 kg (20 minutes before tap)
Mn - 75 %		
C - 6 %		
Si - 1.5 %		
Ladle		
Ferro-manganese	225 kg	300 kg
Ferrosilicon	450 kg	450 kg
Si - 70 %		
Al - 1.25%		
Aluminium (96 % Al.)	18 kg	18 kg
Tapping and Teeming Details		
Tapping time (minutes)	6	5
Teeming time upto hot top junction		
First set (8 moulds of 3.2 t)	4 min. 30 sec.	5 min. 10 sec.
Second set (8 moulds of 2.2 t)	3 min. 20 sec.	3 min. 40 sec.
Third set (8 moulds of 2.2 t)	4 min. 15 sec.	3 min. 45 sec.
Tonnage made (including top poured ingots)	86.9[illegible]	76.36
Ladle skull	1/2 bottom	Bottom

Table I contd...

Composition of refractories, % (Feeder head, Trumpet, Runner, Ladle bricks)	
SiO_2	61 %
Al_2O_3	30 %
Fe_2O_3	2.5%
TiO_2	1.5%
MgO	1.5%
CaO	1.0 %
K_2O	1.0 %
Na_2O	1.5 %

TABLE II - LADLE SAMPLE ANALYSIS

Cast No.	Elements				
	C	Mn	S	P	Si
A 11876	0.56	0.75	0.024	0.022	0.272
A 12997	0.49	0.67	0.023	0.024	0.282
A 17449*	0.51	0.72	0.028	0.034	0.244
A 17746*	0.58	0.66	0.029	0.029	0.282

* Bottom portion of two ingots from these heats was used for detailed investigation.

TABLE III - CHEMICAL ANALYSIS OF BOTTOM POURING COMPOUND

Constituents	%
CaO	16.50
SiO_2	30.80
CaF_2	0.80
Al	0.90
FeO	nil
Fe_2O_3	3.72
C	15.20.
MgO	2.48
Al_2O_3	21.28
P_2O_5	0.21
TiO_2	0.70
Alkali	nil
Water soluble portion	7.40

(Fig.2) was done spectrally (Polyvac) to determine C, Mn, S,P and Si with an ultimate aim of assessing the extent of segregation. The constitution and liquidus temperatures of inclusions were determined from equilibrium diagrams. The scum samples collected from the ingots from various locations were analysed by conventional chemical methods.

RESULTS AND DISCUSSION

Segregation in the bottom portion of ingot

The variation in chemical analysis in C, Mn, S,P and Si at the bottom portion of the ingot at different locations (Fig.2) has been summarised in Table IV. In general, there has been a negative segregation of various elements to a varying degree, at the bottom portion of the ingot (Table IV).

MACROSTRUCTURE OF THE INGOT

The general segregation pattern is shown in Fig.3. Typically there is the central "V" segregation pattern in the top 70% of the ingot.

DISTRIBUTION OF INCLUSIONS

The distribution of oxide and sulphide inclusions in an ingot (Fig.1)

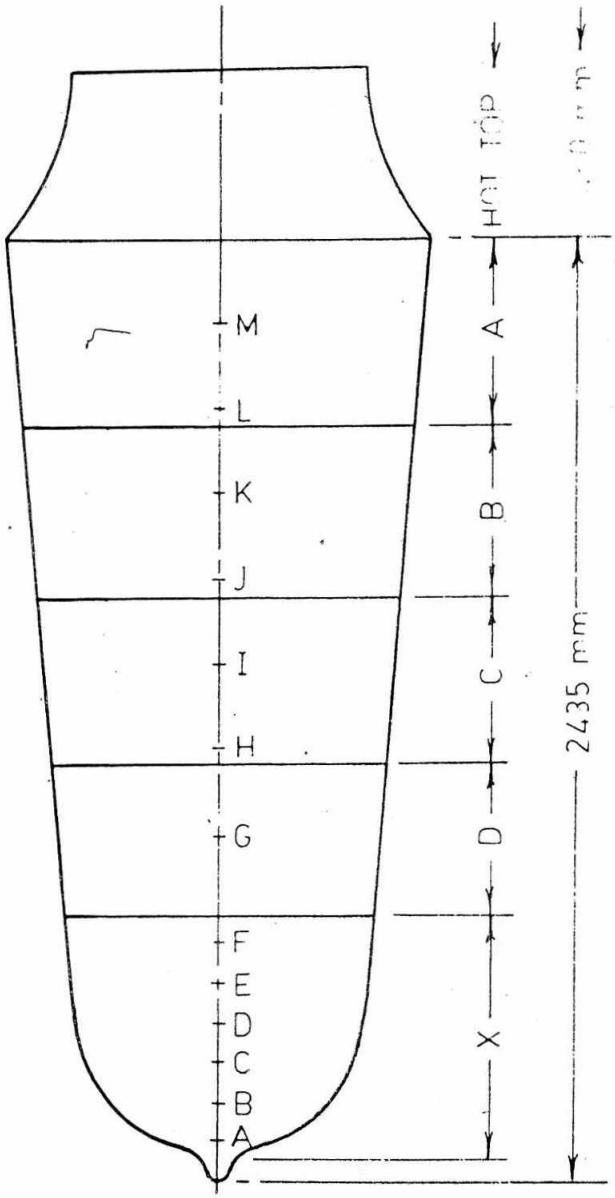

Fig.1 Sampling positions in the ingot.

is shown in Figs.4 and 5 respectively. The average oxide and sulphide inclusions volume fractions in horizontal slices taken from the bottom portion of the ingot are shown in Figs.6,7 and 8 respectively. In all the ingots there is clearly a general segregation of oxides in the bottom portion of the ingots whereas sulphides were segregated in the top region of the ingot. The detailed distribution of the inclusions (Figs.4,6 and 7) showed that there was by no means a uniform distribution of oxides throughout the bottom segregated region. But, in all the ingots a very

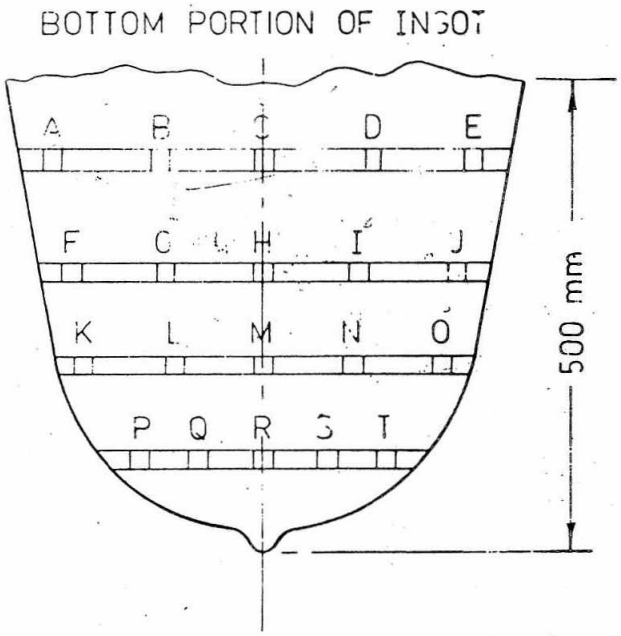

Fig.2 Position of samples taken for chemical analysis.

similar pattern of the inclusion distribution was obtained.

Observations of inclusions in relation to the macrostructure and microstructure

BOTTOM END OF THE INGOT

Inclusions at the bottom end can be classified in two general groups, sulphides and globular silicates. Fig.9(a) is a typical field with these two types of inclusions. The sulphide inclusions in Fig.9(a) have been magnified in Fig.9(b) and a dark phase can be clearly seen in the centre of individual inclusions. The sulphides are obviously of type I indicative of high concentration of dissolved oxygen in the liquid. Type II sulphides were occasionally seen in the bottom end of the ingot and type III sulphides were never observed in this region. The silicate inclusions also clearly indicate the presence of distinctly crystalline phases as shown in Fig.9(c). The electron optical pictures of these two types of inclusions are shown in Figs.9(d) and 9(e). The central dark phases of the sulphide inclusions were analysed as manganese silicates (average analysis MnO - 43% and SiO_2 - 57%, rationalised to no iron basis) and the sulphides were manganese sulphides. The crystalline phases in the silicate inclusions were pure corundum and did

TABLE IV - CHEMICAL ANALYSIS OF SAMPLES COLLECTED FROM BOTTOM PORTION OF INGOTS

Cast No. A 17449 Denoted as X
Cast No. A 17746 Denoted as Y

6

Position of samples corresponding to Fig.2	Elements, %									
	C		Mn		S		P		Si	
	X	Y	X	Y	X	Y	X	Y	X	Y
A	.50	.56	.69	.66	.030	.028	.033	.028	.244	.278
B	.49	.54	.67	.65	.028	.029	.029	.026	.243	-
C	.49	.54	.68	.63	.026	.027	.030	.024	.232	.269
D	.50	.55	.68	.64	.027	.026	.031	.024	.240	.274
E	.51	.57	.70	.64	.028	.027	.032	.026	.240	.274
F	.49	.55	.70	.63	.026	.026	.034	.028	.238	.284
G	.49	.55	.68	.62	.023	.025	.030	.028	.240	.271
H	.47	.53	.69	.60	.022	.028	.029	.027	.234	.269
I	.48	.54	.69	.62	.024	.029	.029	.027	.236	-
J	.49	.56	.70	.62	.024	.030	.033	.029	.237	.269
K	.48	.55	.71	.63	.025	.029	.033	.026	.239	.262
L	.48	.53	.69	.62	.026	.027	.029	.026	.240	.269
M	.47	.54	.70	.62	.023	.026	.030	.023	.238	.268
N	.47	.54	.70	.61	.025	.025	.031	.024	.241	.265
O	.49	.56	.70	.64	.027	.027	.032	.026	.240	.265
P	.48	.54	.71	.63	.028	.026	.033	.026	.241	.281
Q	.48	.52	.70	.64	.027	.024	.031	.027	.240	.280
R	.47	.52	.70	.62	.027	.024	.032	.025	.242	.277
S	.46	.54	.68	.63	.026	.026	.032	.025	.238	.272
T	.47	.55	.69	.63	.026	.026	.032	.027	.237	.277
Average ladle sample analysis	.51	.58	.72	.66	.028	.029	.034	.029	.244	.282

not show the presence of any other element. The matrix silicates of these inclusions were basically calcium-manganese-aluminium silicates with some TiO_2. Average analyses of this phase in different inclusions at the top end and at the bottom end are given in Table V. The volume fraction of Al_2O_3 particles and approximate melting point(42,43) are also given in Table V. The optical, electron optical and X-ray pictures for Fe, Al, Mn and Silicon of one such inclusion are shown in Figs.10(a-f)

The position of the inclusions in the dendritic structure could not be determined by etching with picral or nital. The presence of ferrite did not, necessarily, indicate interdendritic region. Fig.11(a) shows a number of sulphide inclusions in the pearlitic region delineating the last liquid to solidify in the interdendritic area, while the ferrite region hardly shows any sulphides. Fig.11(b) shows a typical silicate inclusion in the ferrite region, a smaller silicate inclusion in the pearlitic region nearby and a sulphide inclusion in pearlite,

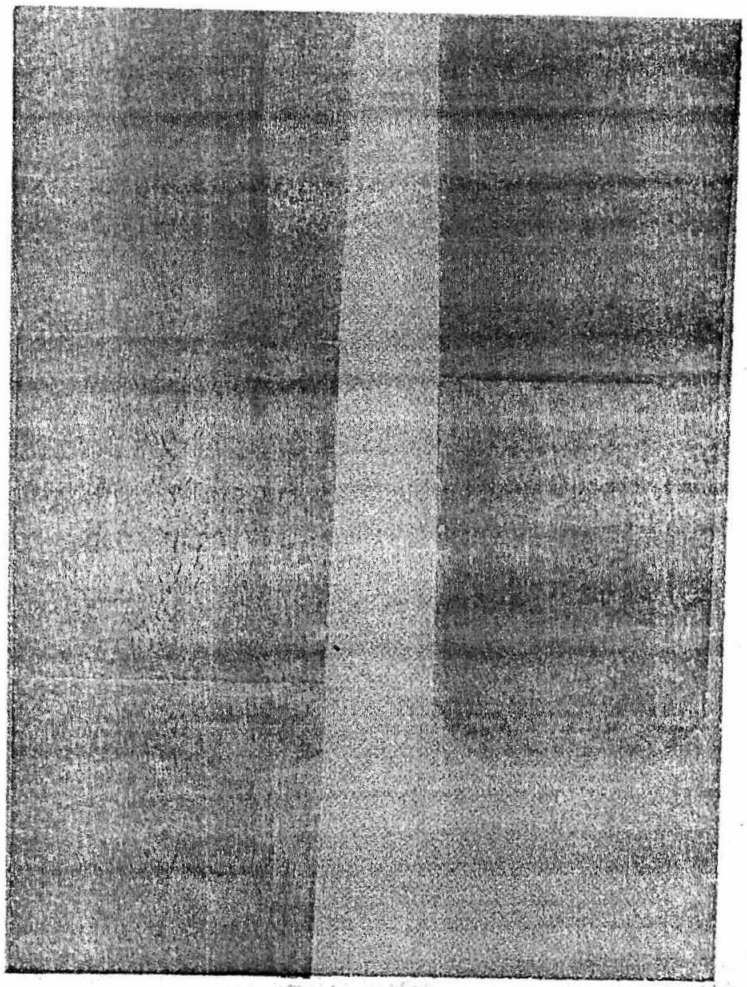

Fig.3 Sulphur prints of ingot sections.

a distance away. Fig.11(c) shows electron optical picture of silicate inclusions in Fig.11(b). Since sulphide inclusions are present in the interdendritic liquid, and the interdendritic zone did not necessarily transform into ferrite, a more positive way of identification of the dendritic structure was required.

The structure of a sample from the bottom end is shown in Fig.12(a) after etching first in nital and then in Stead's reagent. The darker regions correspond to the dendrites, and the lighter areas, the interdendritic liquid. The marked area on this micrograph is magnified in Figs. 12(b) and 12(c), clearly indicating the presence of corundum containing silicate inclusions inside the dendrite arm. The electron optical and the silicon X-ray pictures of the inclusions, shown in Figs.12(d) and 12(e), confirm that these inclusions have the same nature as the typical bottom end inclusions as shown in Figs.9-11. Most of such inclusions were seen inside the dendrite arms, although occasionally these inclusions could be seen in the interdendritic region, as shown in Figs.13 (a-c).

TOP END OF THE INGOT

The inclusions in the top end of the ingot were invariably placed in the interdendritic area as shown in Fig.14. The absence of ferrite delineation of prior austenite boundaries indicate comparatively higher carbon content than those represented by Figs.12(a) and 13(a). The morphology of the sulphide inclusions at the top end is dramatically different from that of sulphides observed at the

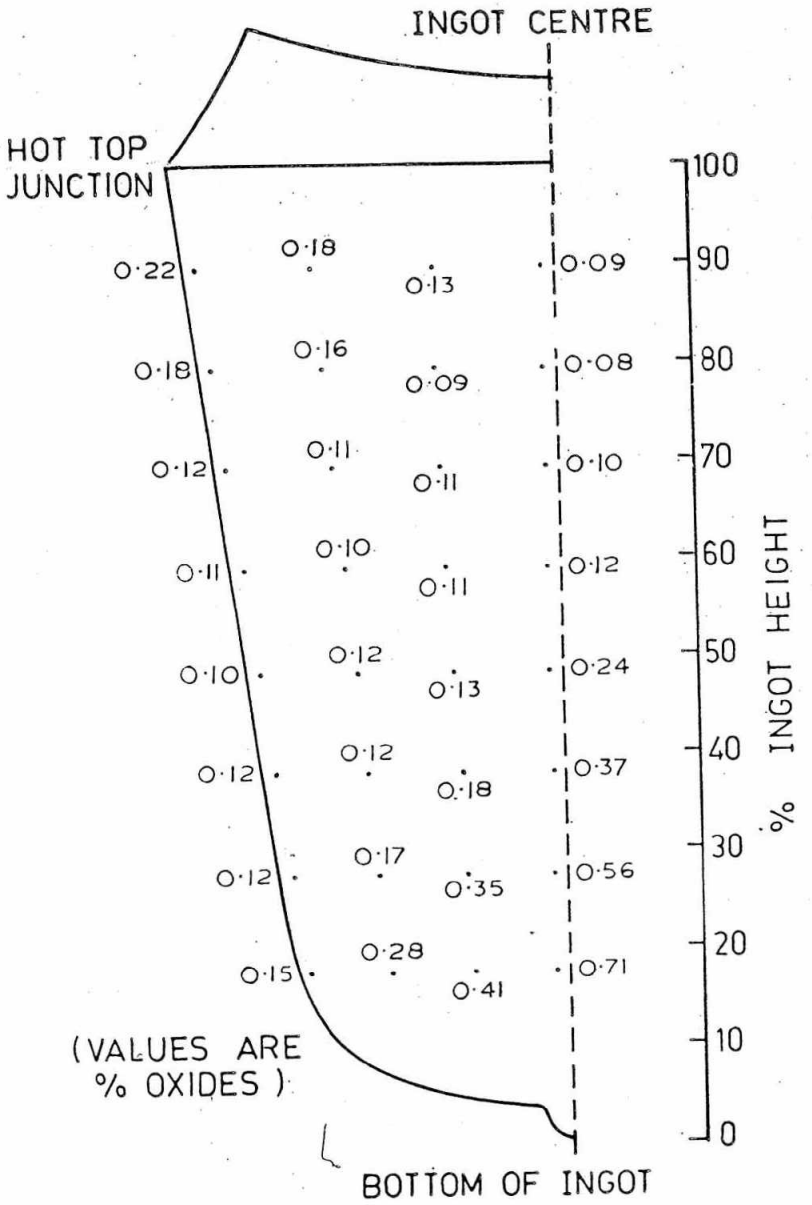

Fig.4 Distribution of oxides in an ingot (Cast No. A 11876).

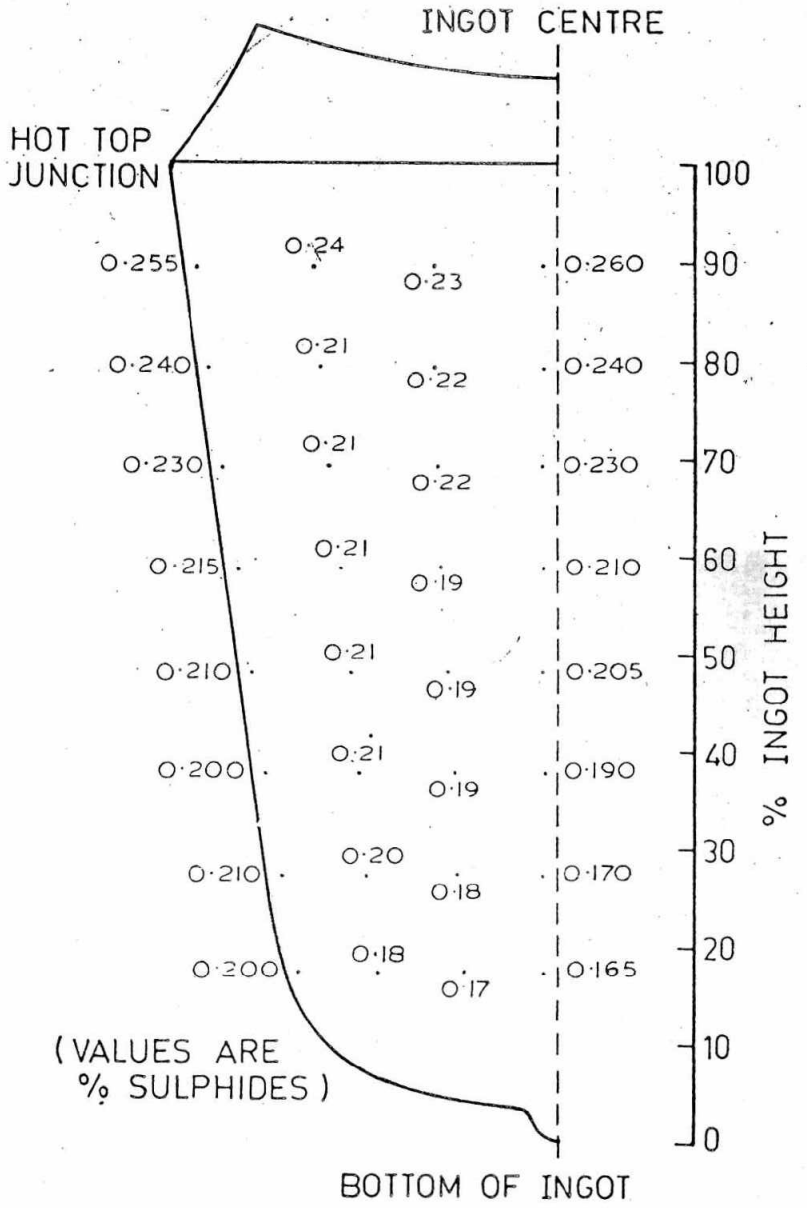

Fig.5 Distribution of sulphides in an ingot (Cast No. A 11876).

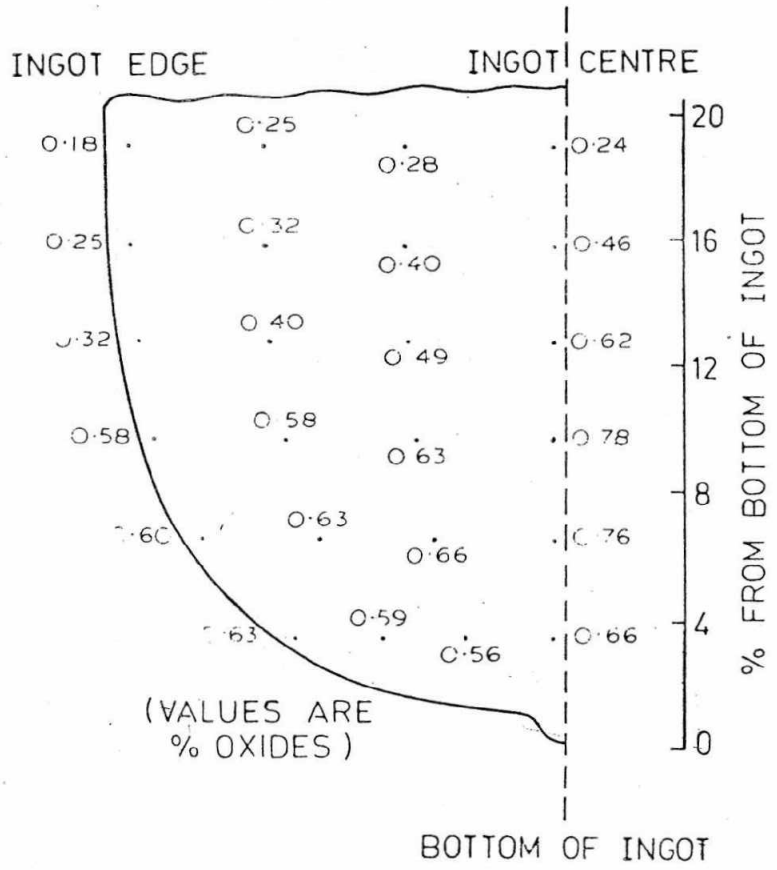

Fig.6 Distribution of oxides in the bottom portion of an ingot (Cast No. A 12939).

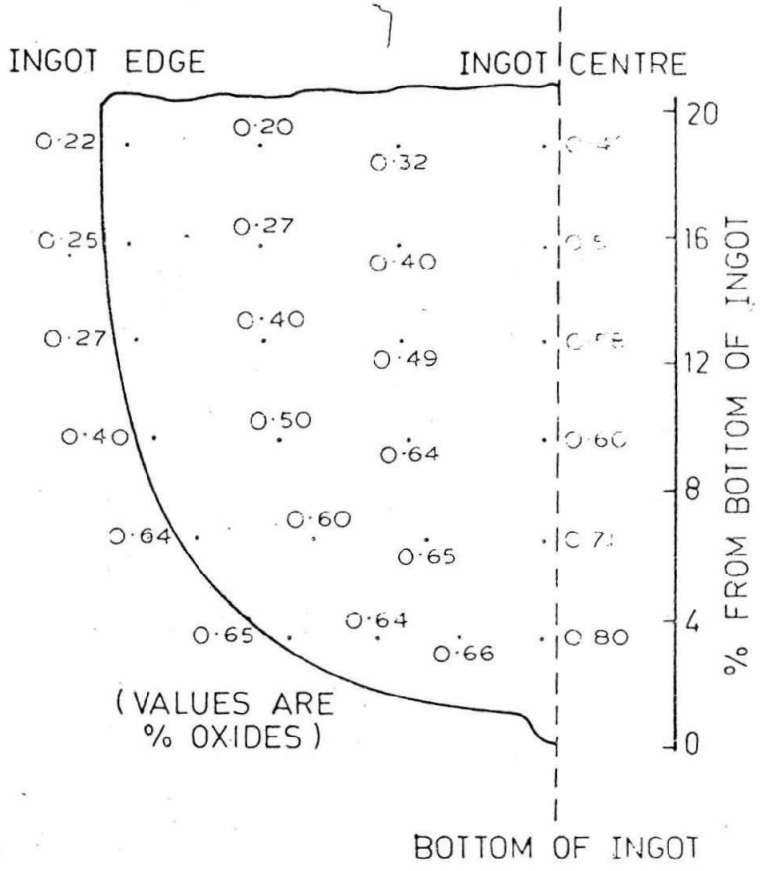

Fig.7 Distribution of oxides in the bottom portion of an ingot (Cast No. A 17449).

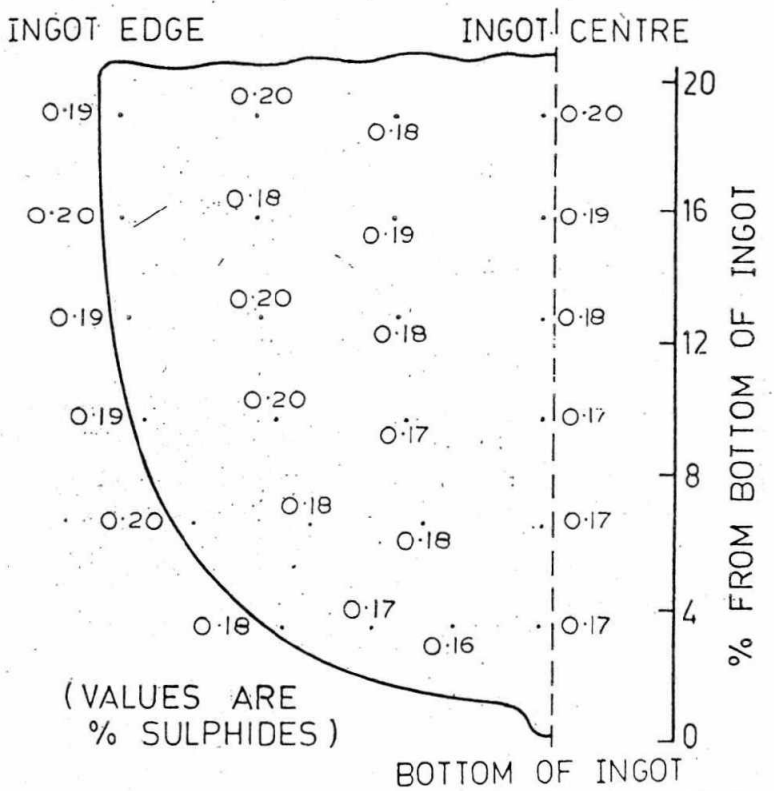

Fig.8 Distribution of sulphides in the bottom portion of an ingot-(Cast No. A 17449).

TABLE V - DETAILS OF INCLUSIONS

	CONSTITUENTS %				
	Al_2O_3	SiO_2	MnO	CaO	TiO_2
Average analysis of silicate matrix					
Top end	19.21	49.59	25.95	2.31	2.92
Bottom end	22.78	47.70	17.75	9.25	1.90
Volume fraction of corundum crystals in the inclusions					
Top end	17.60	-	-	-	-
Bottom end	57.90	-	-	-	-
Weighted average analysis of the inclusions					
Top end	33.43	40.86	21.38	1.90	2.40
Bottom end	67.50	20.08	7.50	3.89	0.80

Estimated Liquidus Temperature, °C	Matrix	Inclusions (weighted average)
Top end	1250	1400
Bottom end	1160	1700

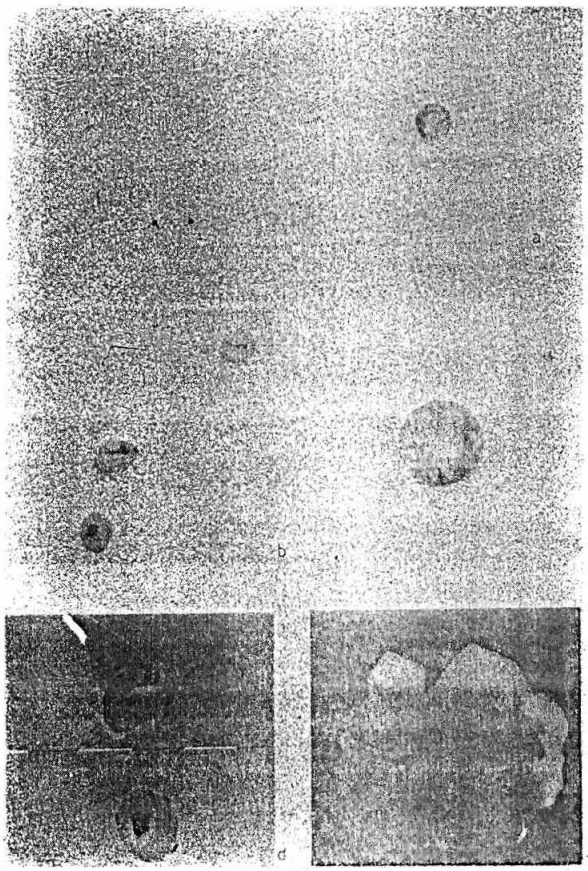

Fig.9(a) Typical inclusions at the bottom of ingot, optical, unetched X 310

(b) Sulphide inclusions in Fig.9(a), optical, unetched X 800

(c) Silicate inclusions in Fig.9(a), optical, unetched X 800

(d) Electron optical picture of sulphide inclusions of Fig.9(a) X 2800

(e) Electron optical picture of silicate inclusions of Fig.9(a) X 2800

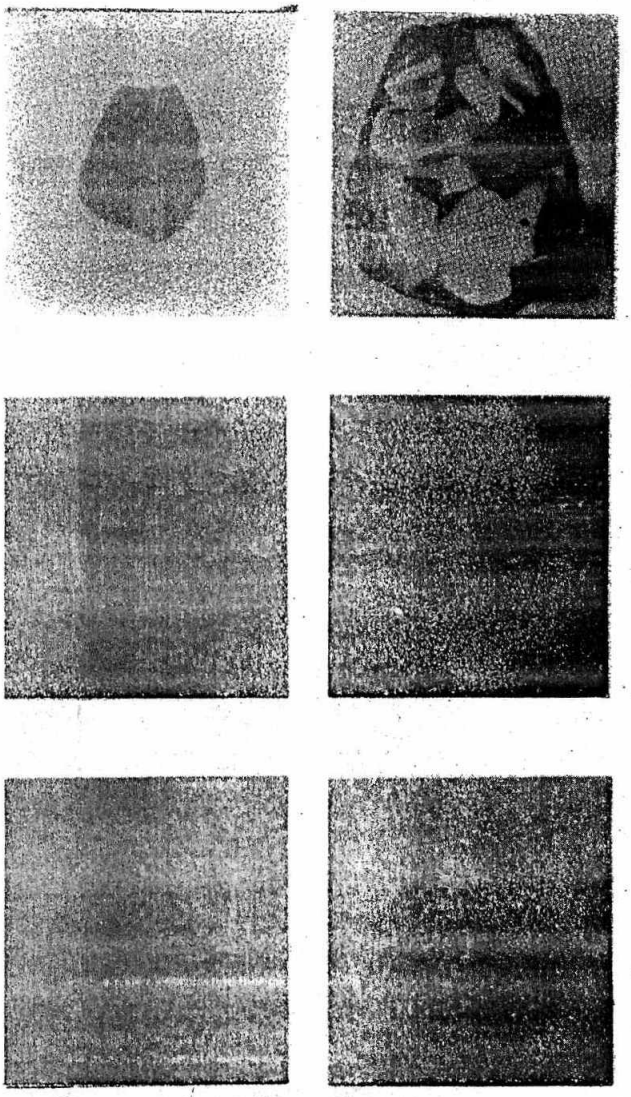

Fig.10 Electron microprobe images of an inclusions in ingot sample (bottom portion - location B - Fig.1)

a - optical micrograph (X 1500)

b - Electron optical micrograph (X 4000) showing pure crystals of Al_2O_3 75.50, SiO_2-21.26, CaO-1.76, MnO-1.17, FeO-0.31) and X-ray images (X 4000) showing concentrations of Fe(e), Al(d), Mn(e) and Si (f).

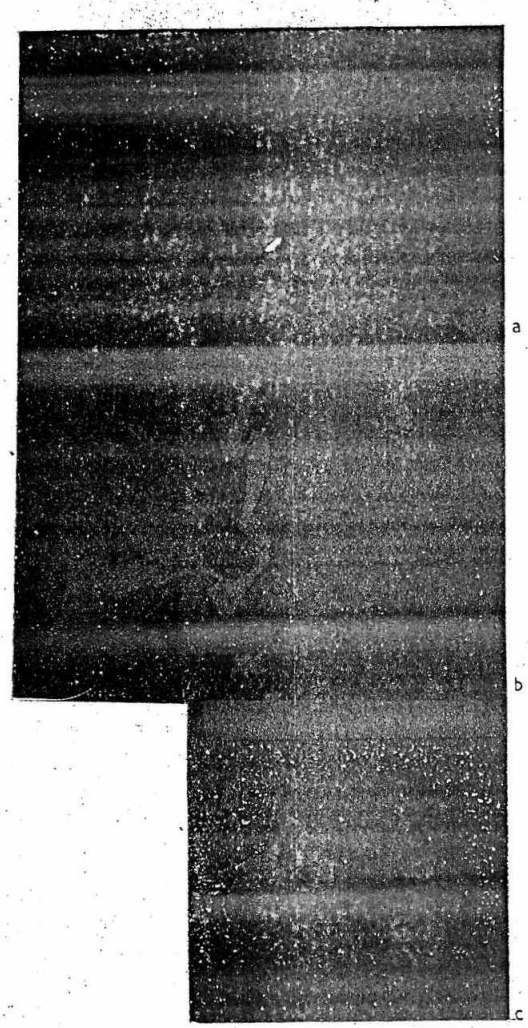

Fig.11(a) Bottom end of ingot - sulphide inclusions delineating inter-dendritic zone in pearlite, etched in nital, optical X 250

(b) Silicate and sulphide inclusions in etched (nital) sample, optical X 360

(c) Electron optical picture of silicate inclusions in Fig. 11(b) X 2650

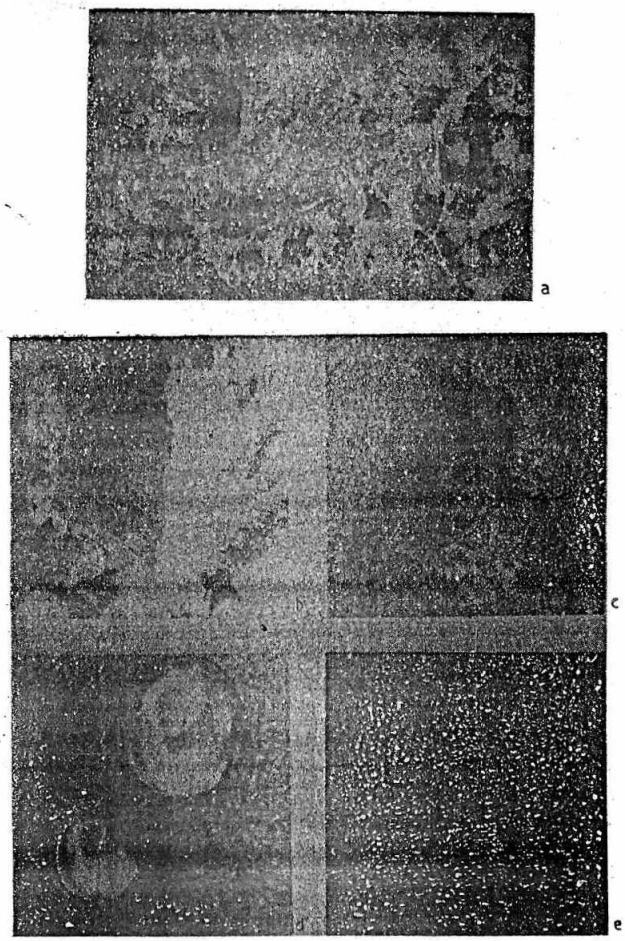

Fig.12(a) Bottom end of ingot-dendritic structure revealed by etching in Stead's reagent, optical X 32

(b) The marked portion of Fig.12(a) has been enlarged. Silicate inclusions can be seen in the dendrite, optical X 125

(c) Silicate inclusions of Fig. 12(b), marked area have been magnified, Optical X 750

(d) Electron optical picture of the silicate inclusions X 2800

(e) Si X-ray picture of the silicate inclusions. Shows voids in areas of corundum crystals X 750

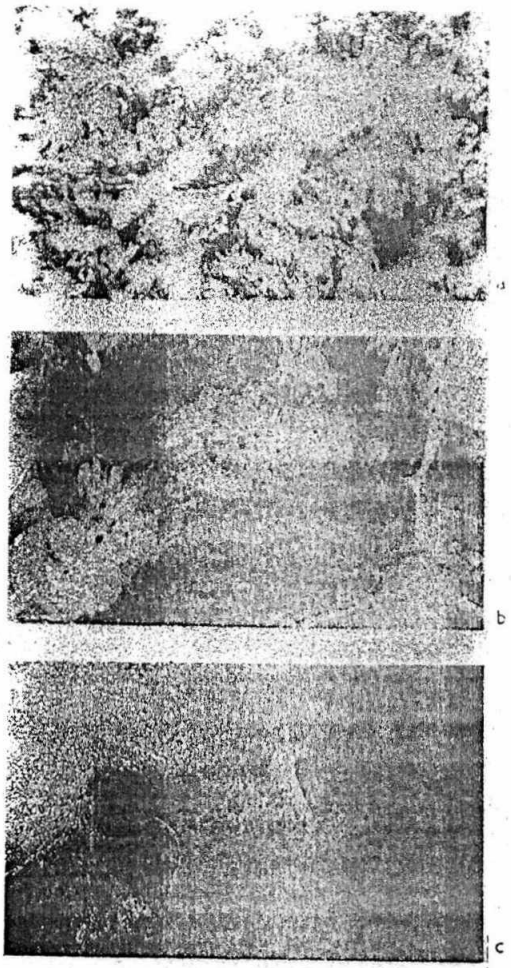

Fig.13 (a) Bottom end of ingot-dendritic structure revealed by etching in Stead's reagent, optical X 32

(b) Marked area of Fig.13(a), inclusions in interdendritic region, optical X 125

(c) Marked area of Fig.13(b), silicate and sulphide inclusions, Optical X 750

bottom end. The sulphides at the top end, Figs.15(a) and 15(b), are of type II or type III, being mostly of the later type in the top central region. The sulphides are clear indication of low concentrations of dissolved oxygen. The presence of type II or type III sulphides in the highly segregated top central portion of the ingot also indicates that while this area has been enriched with carbon, sulphur and phosphorus during the progress of solidification, it has been systematically denuded of oxygen.

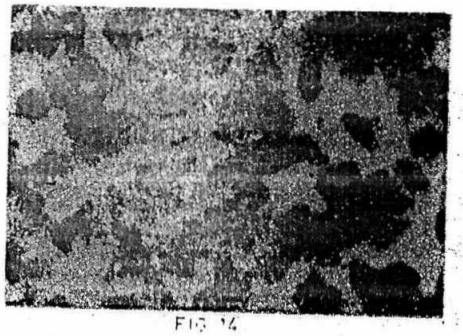

FIG 14

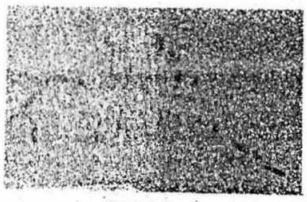

FIG 15 (a)

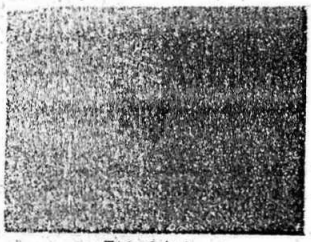

FIG.15 (b)

Fig.14 Top end of ingot-inclusions in interdendritic region, etched in Stead's reagent, optical X 32

Fig.15(a) Type II sulphides at top end, unetched, optical X 1100

Fig.15(b) Type III sulphides at top end, unetched, optical X 1100

It is possible that oxygen precipitates out, as oxides, with the progress of solidification, and these oxides are swept away from this region, either by convection or by the falling dendrites of equiaxed crystals. The concentration of dissolved oxygen in the interdendritic fluid continuously drops because of oxide formation, while the concentration of elements like carbon, sulphur and phosphorus increases, because of their solubility in the remaining liquid.

The oxide inclusions seen in the top end of the ingot are considerably bigger than those seen at the bottom end. They are basically of two types (a) corundum containing silicates,

and (b) alumina clusters. These oxide inclusions were always seen in the interdendritic region. A large silicate type inclusion is shown in Fig.16. An area of alumina clusters is shown in Figs.17(a) and 17(b). The alumina inclusions were often associated with manganese sulphide inclusions, as can be clearly seen in Fig.17(b). It may be noted that these sulphides are of type III, casting doubts on the general belief that type III sulphides always occur as single phase inclusions. Even the large corundum bearing silicate inclusions were often associated with some sulphides; similar inclusions seen at the bottom end were not associated with sulphides. The presence of high melting point alumina clusters and the corundum bearing silicate inclusions in the interdendritic region, the large size of these alumina clusters and the inclusions and their co-existence with type III sulphides (Figs.18 a-c) indicates that these oxides have been transported into this area of low oxygen liquid during the progress of solidification.

MECHANISM OF FORMATION OF THE BOTTOM CONE OF INCLUSIONS AND BOTTOM CONE OF NEGATIVE SEGREGATION

The bottom end of the ingot has shown negative segregation (Table IV) and also the bottom cone of inclusions (Figs.4,6 and 7). It is highly likely that the mechanism of formation of the bottom cone of oxide inclusions and that of the bottom cone of negative segregation is related.

The presence of CaO in the inclusions suggests entrapment of bottom pouring flux and/or slag. Since the MgO content of the inclusions was negligible and since the open hearth slag contains 6% MgO (Table 1), contribution from this slag can be considered to be insignificant. Presence of TiO_2 suggests incorporation of croded refractory in the inclusions; the TiO_2 content of the refractory was 1.5-2%. The weighted average analysis of inclusions at the bottom end showed 67.50% Al_2O_3. None of the exogenous sources e.g. slag, bottom pouring compound, refractory had such high percentage of Al_2O_3, It can be concluded, therefore, that Al_2O_3 particles formed as a result of primary deoxidation are incorporated in these inclusions. A striking difference in the position of corundum

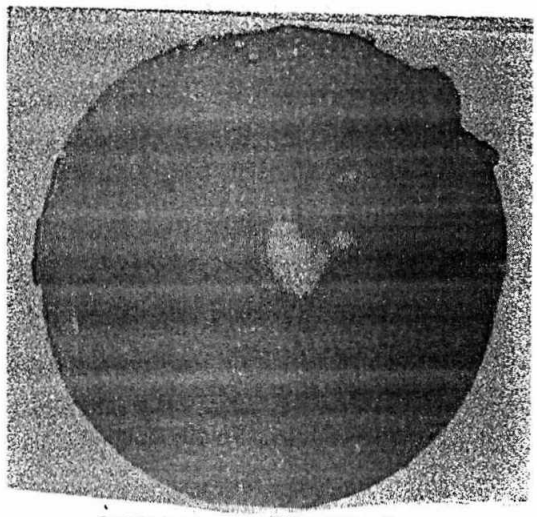

OPTICAL MICROGRAPH

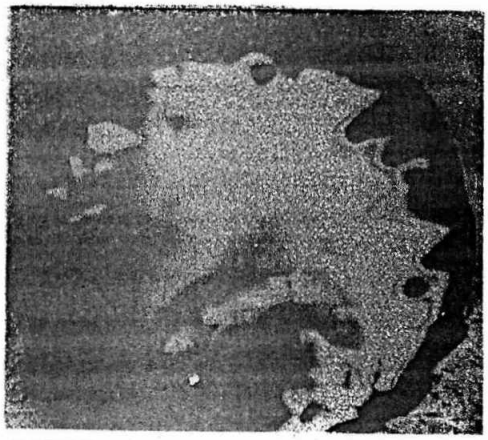

ELECTRON OPTICAL MICROGRAPH

Fig.16 Top end of ingot - a large silicate inclusion X 800

crystals, i.e. the inclusions at the bottom end and in inclusions at the top end, has been noticed; the corundum crystals are at the central region in the bottom end inclusions suggesting nucleation of silicates around Al_2O_3 while they are at the surface in the top end inclusions, suggesting precipitation from liquid. The increase in the MnO and SiO_2 content in the inclusions at the top part of the ingot, which solidified at the end, is a result of deoxidation during solidification.

Since primary deoxidation products like Al_2O_3 are present along with a silicate matrix with high CaO, it can be concluded that the inclusions ultimately at the bottom end were present in the liquid in the early stages of solidification. Further the presence

TABLE VI - TOTAL ALUMINIUM CONTENT IN EXPERIMENTAL INGOTS

Cast No.	Total aluminium content, %		
	Top region	Middle region	Bottom region
A 12997			
(a) Ingot corresponding to first set.	0.010	0.017	0.024
(b) Ingot corresponding to third set	0.009	0.014	0.020
A 17449			
(a) Ingot corresponding to first set	0.010	0.018	0.028
(b) Ingot corresponding to second set	0.010	0.016	0.024

TABLE VII - CHEMICAL ANALYSIS OF SCUM*

Constituents, %	Plate I (First set)			Plate II (Second set)			Plate III (Third set)		
	Top	Middle	Bottom	Top	Middle	Bottom	Top	Middle	Bottom
CaO	8.9	8.7	8.6	9.1	8.8	8.7	9.5	8.8	8.5
SiO_2	44.6	41.7	40.1	46.4	43.5	40.4	48.1	43.9	41.8
Al_2O_3	26.4	32.7	35.6	26.3	32.6	34.8	25.8	31.9	33.9
Fe_2O_3	6.85	6.32	6.12	6.21	5.85	5.63	5.86	5.81	5.43
$Na2O + K_2O$	nil	nil	nil	nil	nil	nil	nil	nil	nil
MnO	0.60	0.75	0.93	0.85	1.10	1.19	0.97	1.20	1.31
MgO	2.96	2.67	2.62	2.78	2.65	2.67	2.24	2.26	2.17
TiO_2	0.87	0.82	0.76	0.79	0.73	0.66	0.75	0.71	0.68
P_2O_5	.175	.180	.180	.180	.176	.174	.181	.174	.174
Ignition loss	4.00	3.90	3.60	3.50	3.10	2.80	3.20	2.90	2.60
CaF_2	nil	nil	nil	nil	nil	nil	nil	nil	nil

* Metallic iron (1-3 %) was also present in the scum, more at bottom levels and less at top levels.

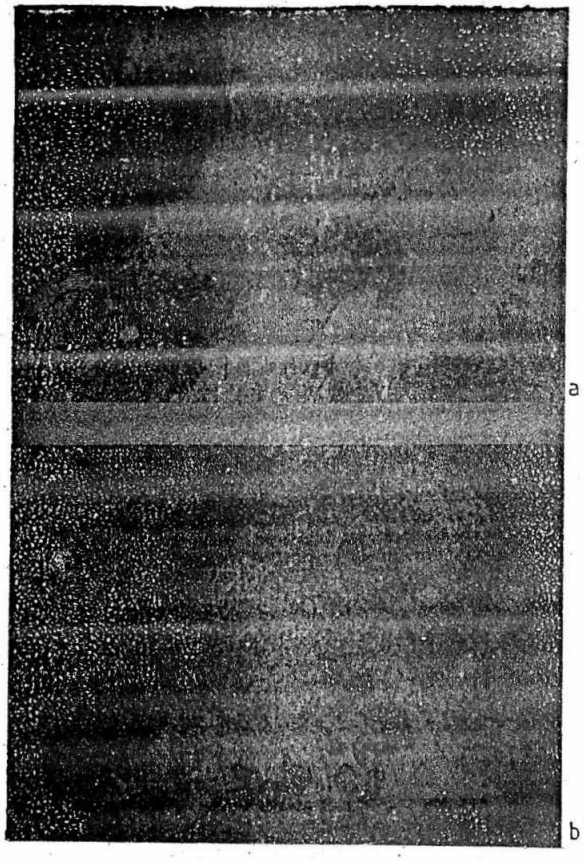

Fig.17(a) Top end of ingot - oxide clusters in the interdendritic area, etched in Stead's reagent, marked area of Fig.14, optical X 110

(b) Top end of ingot-alumina inclusions in clusters are clearly associated with sulphides, marked area of Fig.17(a), optical X 660

of these inclusions inside the dendrite arms clearly indicates either nucleation of equiaxed crystals on these inclusions or incorporation of the inclusions in the growing dendrites of equiaxed crystals. It is clear, therefore, that the bottom cone of negative segregation is associated with high concentration of high melting point oxide inclusions like those rich in Al_2O_3 which although separated from liquid steel as liquid inclusion, perhaps, solidify and become integral parts of the dendrites formed. It will, of course, be more accurate to describe these inclusions, not by their melting points but by the liquidus temperature. The first inclusions to be dragged down will be those of highest

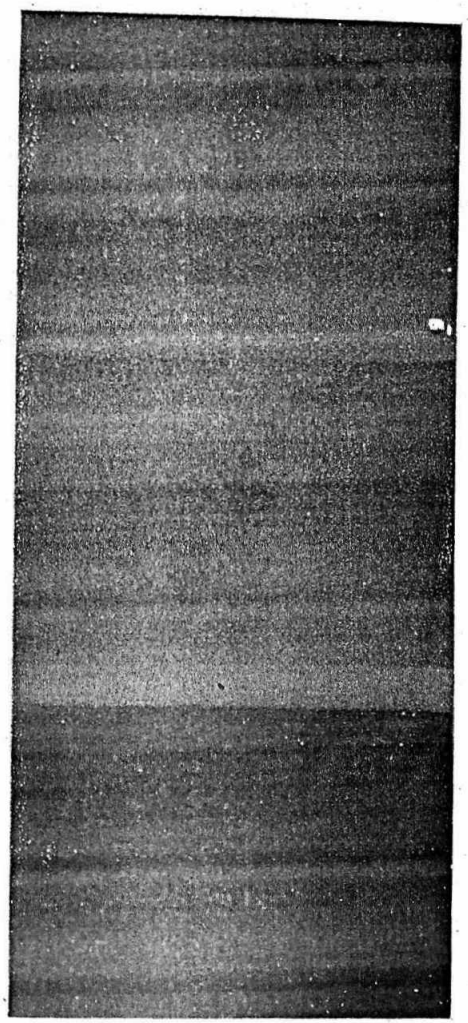

Fig.18(a) Top end of ingot-alumina clusters with type III sulphides, optical X 720

(b) Electron optical picture of inclusions in Fig.18(a) X 960

(c) Details of alumina and sulphide in the inclusions shown in Fig. 18(b) electron optical X 3750

liquidus temperature above that of steel, in which solid particles of alumina have already separated. This observation has further been confirmed by the increase of total aluminium content of steel from top to bottom end (Table VI) and also by the analysis of scum which shows that alumina pick up in the bottom pouring flux is more at the bottom end than at the top end (Table VII). Since some of these inclusions are also seen in the inter-

dendritic region in the bottom and top end of the ingot, it is unlikely that they nucleated the equiaxed grains.(22) These inclusions separated as liquid silicates are never seen in the spine of the dendrites. This explains why many of the silicate inclusions shown by Franklin and Evans(33) were actually in the interdendritic region. The presence of type I sulphides in the bottom end of the ingot indicates early solidification, when the concentration of dissolved oxygen in the liquid was relatively high.

CONCLUSIONS

(i) The bottom cone of oxide inclusions is a result of incorporation of these inclusions in the dendrites of equiaxed grains. The inclusions drop to the bottom end with the shower of relatively pure equiaxed grains.

(ii) The last-to-solidify interdendritic fluid is enriched in carbon, sulphur and phosphorus but is denuded of oxygen. The first three elements having high solubility in the interdendritic fluid do not form precipitates, but oxygen concentration cannot increase with the progress of solidification because of precipitation of oxides due to low solubility.

(iii) The low concentration of soluble oxide and the presence of large oxide inclusions and alumina clusters in the interdendritic region at the top end of the ingot indicate significant movement of the interdendritic fluid towards the top end during the progress of solidification.

ACKNOWLEDGEMENT

The authors thank the Management of The Tata Iron and Steel Company Limited, for permission to publish this paper. Thanks are also due to Prof.G.J.Davies, Department of Metallurgy, The University of Sheffield for providing facilities for carrying out metallographic study and for financial assistance to one author(T.M) and to Dr.D.H.Krikwood of Sheffield University for helpful discussions.

REFERENCES

1. M.C.Flemings, D.R.Poirier,R.V. Barone and H.D.Brody: J.Iron Steel Inst.,1970,208,371-381.
2. E.Scheil: Z.Metalek,1942,34,70-72.
3. W.Steven and D.R.Thorneycorft: J. Iron Steel Inst.,1957,187,15-32.
4. D.A.Melford and D.A.Granger: The Solidification of Metals,289-294; 1968,London, The Iron and Steel Institute.
5. T.Z.Kattamis and M.C.Flemings: Trans.AIME,1965,233,992-999.
6. M.C.Flemings: Modern Castings, 1964,46,353-362.
7. R.D.Doherty and O.A.Melford: J. Iron Steel Inst.,1966,204,1131-1143.
8. G.J.Davies: 'Solidification and Casting', 117-122;1973,London, Applied Science Publishers Ltd.
9. G.S.Cole and G.F.Bolling: Trans. AIME,1966,236,149-158.
10. L.F.Donaghey and W.A.Tiller: 'The Solidification of metals',87-92; 1968,London, The Iron and Steel Institute.
11. K.G.Lewis: Iron and Coal Trades Review,1955,125-32,189-96,251-56, 309-14,381-87,437-42.
12. H.Biloni and G.F.Bolling: Trans. AIME,1963,227,1351-1360.
13. J.J.Kramer,G.F.Bolling and W.A. Tiller: ibid.,374-381.
14. R.F.Polich and M.C.Flemings: Trans. AFS,1965,73,1-13.
15. R.Mehrabian, M.Keane and M.C. Flemings: Metall. Trans.,1970,1, 1209-1220.
16. M.C.Flemings and G.E.Nereo: Trans. AIME,1967,239,1449-1461.
17. M.C.Flemings, M.C.Mehrabian and G.E.Nereo: ibid.,1968,242,50-55.
18. M.C.Flemings,R.Mehrabian and G.E. Nereo: ibid.,41-49.
19. R.J.Mc Donald and J.D.Hunt: ibid, 1969,245,1993-1997.
20. A.Kohn: 'The solidification of Metals',356-362; 1968,London, The Iron and Steel Inst.

21. K.A.Jackson, J.D.Hunt,D.R. Uhlmann end T.P.Seward: Trans. AIME,1966,236,149-158.

22. P.H.Salmon-Cox and J.A.Charles: J.Iron Steel Inst.,1963,201, 863-872.

23. P.H.Salmon - Cox and J.A.Charles: ibid,1965,203,493-499.

24. A.Ohno: 'The Solidification of Metals',349-356;1968;London,The Iron and Steel Institute.

25. T.Z.Kattamis,U.T.Holmberg and M.C.Flemings: J.Metals,1967, 239,1504-1511.

26. R.Mehrabian and M.C.Flemings: Metall. Trans.,1970,1,455-464.

27. T.F.Bower, H.D.Brody and M.C. Flemings: ibid,1966,236,624-634.

28. J.S.Kirkaldy and W.V.Youdelis: ibid.,1958,212,833-840.

29. F.Weinberg,J.Lait and R.Pugh: 'Solidification and casting of Metals',334-339;1977,London, The Iron and Steel Institute

30. R.Mehrabian, M.Keane and M.C. Flemings: Metall. Trans.,1970,1, 1209-1220.

31. S.Copley and A.F.Giamei,S.M. Johnson and M.F.Hornbecker: ibid., 2193-2204.

32. G.W.Delamore and N.J.Cavaghan: Interim Report on wax model experiments on segregation in ingot,United Companies Ltd., 1st March 1962.

33. A.G.Franklin and D.H.Evans: J. Iron Steel Inst.,1971,209,369-379.

34. British Patent No.862777,5th July,1967.

35. N.Standish: Iron and Steel, 1969,42,354-360.

36. J.R.Blank and F.B.Pickering: 'The Solidification of Metals' 370-376;1968,London, The Iron and Steel Institute.

37. M.D.Maheshwari and T.Mukherjee: Trans.Indian Inst.Metals,1976, 29(5),322-328.

38. M.D.Maheshwari and T.Mukherjee: Tisco Technnical Journal,1979, 26(1),9-18.

39. M.D.Maheshwari and T.Mukherjee: Trans.Indian Inst.Metals,1976, 29(4),249-253.

40. M.D.Maheshwari and T.Mukherjee: ibid.,1980,33(3),241-245.

41. C.Holden, J.M.Young,P.E. Eldridge and T.W.Deakin: 'Production and Application of Clean Steels',167-176;1972, London, The Iron and Steel Institute.

42. R.Kiessling and N.Lange: 'Non-metallic inclusions in steel', (I),7-43;1964,London, The Iron and Steel Institute.

43. A.Muan and E.F.Osborn: 'Phase equilibria among oxides in steel making', 103-158;1965, Reading, Mass.,Addison-Wesley.